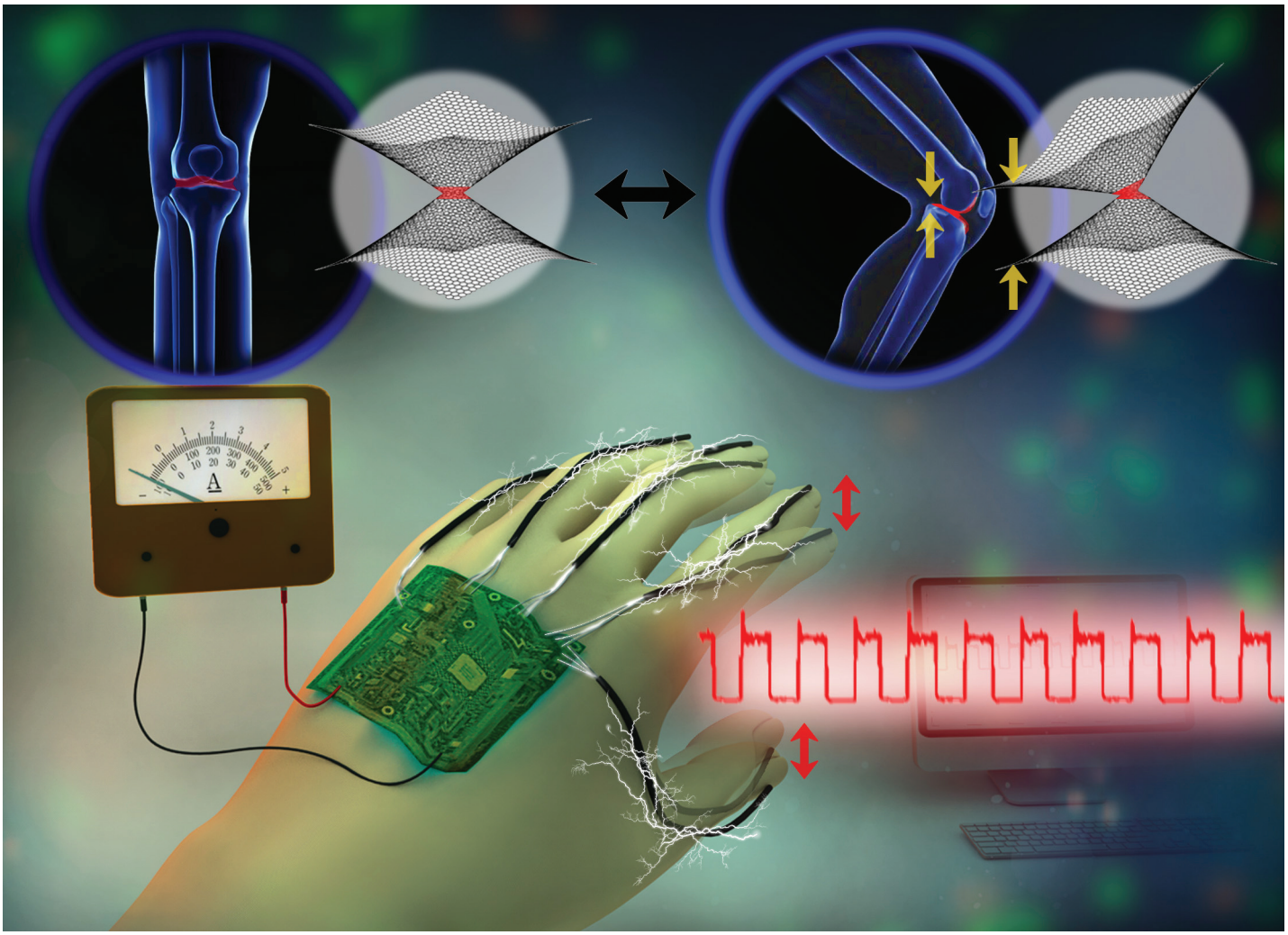

Showcasing research from the Ho Seok Park's group (Energy Storage and Environmental Materials Lab) at the School of Chemical Engineering, Sungkyunkwan University (SKKU), Republic of Korea.

Cartilage-inspired superelastic ultradurable graphene aerogels prepared by the selective gluing of intersheet joints

The cartilage-inspired, selectively bonded viscoelastic poly(dimethylsiloxane) (PDMS) components provided the restorative force that converts fragile three-dimensional (3D) graphene networks into superelastic and ultradurable 3D graphene aerogels (GA). Owing to the combination of excellent mechanical and electrical properties, the GA@PDMS nanocomposites were used as signal transducers for strain sensors, showing very short response and recovery times (in the millisecond range) with reliable sensitivity and extreme durability.

As featured in:

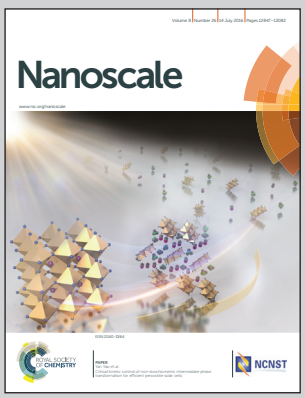

See Jing Kong, Ho Seok Park *et al.*, *Nanoscale*, 2016, **8**, 12900.

ROYAL SOCIETY OF CHEMISTRY

www.rsc.org/nanoscale

Registered charity number: 207890

Nanoscale

PAPER

View Article Online
View Journal | View Issue

CrossMark click for updates

Cite this: *Nanoscale*, 2016, **8**, 12900

Cartilage-inspired superelastic ultradurable graphene aerogels prepared by the selective gluing of intersheet joints†

Jin-Yong Hong,[a,b] Sol Yun,[a] Jeong Jae Wie,[c] Xu Zhang,[d] Mildred S. Dresselhaus,[d] Jing Kong*[b] and Ho Seok Park*[a,e]

In this study, we demonstrate a cartilage-inspired superelastic and ultradurable nanocomposite strategy for the selective inclusion of viscoelastic poly(dimethylsiloxane) (PDMS) into graphene sheet junctions to create effective stress-transfer pathways within three-dimensional (3D) graphene aerogels (GAs). Inspired by the joint architectures in the human body, where small amounts of soft cartilage connect stiff (or hard) but hollow (and thus lightweight) bones, the 3D internetworked GA@PDMS achieves synergistic toughening. The resulting GA@PDMS nanocomposites exhibit fully reversible structural deformations (99.8% recovery even at a 90% compressive strain) and high compressive mechanical strength (448.2 kPa at a compressive strain of 90%) at repeated compression cycles. Owing to the combination of excellent mechanical and electrical properties, the GA@PDMS nanocomposites are used as signal transducers for strain sensors, showing very short response and recovery times (in the millisecond range) with reliable sensitivity and extreme durability. Furthermore, the proposed system is applied to electronic scales with a large detectable weight of about 4600 times greater than its own weight. Such bio-inspired cartilage architecture opens the door to fabricate new 3D multifunctional and mechanically durable nanocomposites for emerging applications, which include sensors, actuators, and flexible devices.

Received 9th March 2016,
Accepted 18th May 2016

DOI: 10.1039/c6nr01986b

www.rsc.org/nanoscale

Published on 19 May 2016. Downloaded by MIT Library on 27/06/2017 20:37:01.

Introduction

Polymer nanocomposites, where nanofillers are included as minor components (< 10 wt% in general), have been investigated to reinforce them due to the nanoscale effect on surface-area-to-volume-ratio and to realize the full functionality potential of expensive and heavy inorganic fillers used as little as possible for low-cost lightweight and functional materials.[1–6]

In sharp contrast to the traditional understanding of mechanical integrity and/or functionality of polymer nanocomposites, nature often offers different strategies for materials design. For instance, nacre contains 95 wt% of hard ceramics (aragonite) combined with 5 wt% of soft organic materials (proteins and polysaccharides), which act as "mortar" rather than a matrix "brick".[7–10] Such a composition (hierarchically architectured in a manner opposite to that for synthetic polymer nanocomposites; these will hereinafter be referred to as inversed nanocomposites) is believed to resolve the bottleneck associated with mechanical properties by a simultaneous enhancement of the material tensile strength and toughness.

Having been inspired by biomimetic materials, strong composites obtained by the integration of graphene or similarly layered 2D nanosheets (used as major hard building blocks) with soft organic materials have been recently demonstrated to achieve synergistic toughening through the interfacial interaction between the basal planes of the nanosheets and the organic components. Such integrated graphene-based composites were fabricated by various methods including layer-by-layer assembly, vacuum filtration, ice-templating, and sintering.[11–14]

Unfortunately, interactions along the lateral direction of nanosheets cannot often improve the mechanical integrity of three-dimensional (3D) graphene aerogels (GAs), in which the edge-to-edge interactions at nanosheet joints are more critical for reinforcing the crack propagation points of intersheet junctions. As has been previously reviewed by the authors and

[a]School of Chemical Engineering, Sungkyunkwan University, Suwon 440-746, Korea. E-mail: phs0727@skku.edu; Fax: +82 31 290 7272; Tel: +82 31 299 4706
[b]Department of Electrical Engineering and Computer Science, Massachusetts Institute of Technology, 77 Massachusetts Avenue, Cambridge, MA 02139, USA. E-mail: jingkong@mit.edu; Fax: +1 617 324 5293; Tel: +1 617 324 4068
[c]Department of Polymer Science and Engineering, Inha University, Incheon 420-751, Korea
[d]Department of Physics, Massachusetts Institute of Technology, 77 Massachusetts Avenue, Cambridge, MA 02139, USA
[e]Department of Health Sciences and Technology, Samsung Advanced Institute for Health Sciences and Technology (SAIHST), Sungkyunkwan University, 2066, Seobu-ro, Jangan-gu, Suwon 440-746, Korea
† Electronic supplementary information (ESI) available. See DOI: 10.1039/c6nr01986b

This journal is © The Royal Society of Chemistry 2016

Published on 19 May 2016. Downloaded by MIT Library on 27/06/2017 20:37:01.

other researchers, 3D macroscopic GA materials possess prominent features such as low densities, highly exposed surface areas, low mass and ion transport resistance, percolation-type electrical conductivity, and good chemical stability; these make them potentially suitable for various applications including electrodes, catalytic supports, absorbents, separators, and chemical/bio-sensors.[15–20] However, weak van der Waals interactions at the graphene sheet junctions result in mechanical integrity issues (such as easy irreversible deformation upon applied stress).[21–24]

For the purpose of overcoming these challenges, various attempts have been performed, such as edge-to-edge assembly,[25,26] introduction of a carbon linker,[27] 3D printing technique,[28] and addition of polymeric segments (*e.g.* polypyrrole (PPy),[29,30] poly(vinyl alcohol) (PVA),[31] poly(acrylic acid) (PAA),[32] poly(dimethylsiloxane) (PDMS),[33,34] *etc.*[35]).

Several approaches demonstrated impressive achievements in mechanical properties (over 90% of compressibility). However, there still remains a challenge to further develop high performance 3D GAs which can simultaneously ensure mechanical and electrical properties. For instance, excessive addition of polymers onto the basal planes of nanosheets can inherently produce detrimental effects on their recovery rates due to the timescale of polymer relaxation as well as on electrical conductivity because of the polymer insulating properties. The selective insertion of soft segments exclusively into graphene intersheet joints is more desirable for the 3D macroscopic GAs since it creates an effective load transfer pathway throughout the interconnected graphene networks by delocalizing the applied stress.

Herein, we demonstrate for the first time cartilage-inspired designs of 3D superelastic and ultradurable GAs that preserve the electrical conductivity of the material. Analogous to the inversed nanocomposite composition, which is found in the human body at the macroscale level, the presence of small amounts of soft cartilage in joints is essential for connecting stiff (or hard) but hollow (and thus lightweight) bones and, hence, building an effective load-bearing system. Such bio-inspired cartilage architecture can be obtained inside the 3D internetworked GAs by selectively gluing the intersheet joints with soft materials and is completely different from the previously studied graphene nanosheet-based artificial nacres with different interaction modes (in-plane interactions *vs.* edge-to-edge interactions).

Experimental section

Synthesis of chemically converted GA

2.0 mg mL^{-1} of the graphene oxide (GO) solution, hypophosphorous acid (H_3PO_2) and iodine (I_2) were mixed (weight ratio of aqueous GO solution : H_3PO_2 : I_2 is 1 : 100 : 10) in a cylindrical vial at 80 °C for 8 h. After gel formation, the chemically converted graphene wet-gel was taken out, washed until pH 7, and freeze-dried into the GA.

Fabrication of the GA@PDMS nanocomposite

The PDMS (Sylgard 184, Dow Corning) was diluted in *n*-hexane. After synthesis of the GA, a diluted PDMS solution (0.5 wt% in *n*-hexane) was infiltrated into the GA by capillary force and thermally cured for 60 min in an oven held at 80 °C.

Characterization

The morphology was confirmed using a Field Emission Scanning Electron Microscope (FE-SEM, JEOL-6700). The TGA curves were acquired from 25 to 800 °C using argon (Ar) as a purge gas with a heating rate of 10 °C min^{-1}. FT-IR spectra were recorded on FT/IR-6100 (Jasco, Japan) from 500 to 4000 cm^{-1}. Raman spectroscopy was recorded on a Jobin Yvon/HORIBA spectrometer equipped with a charge-coupled device (CCD) camera (1024 × 256 pixels). The XPS spectra were obtained using AXIS-Ultra DLD with Al Kα (1486.6 eV). The mechanical properties were characterized by using a TA Instruments dynamic mechanical analyzer (DMA, RSA3) by compression under ambient conditions. The compressive stress–strain response was measured at a strain rate of 0.05 mm s^{-1}. All electrical measurements were conducted with an Agilent Semiconductor Parameter Analyzer (4155C). A constant voltage (100 mV) is applied between the top and bottom electrodes of the sample, and the current is measured and recorded in a sequential mode (with a time interval of 1 second).

Results and discussion

Biomimetic formation of GA@PDMS nanocomposite

The chemically converted GA was readily achieved *via* self-assembly of GO sheets as has been previously reported (ESI†).[36–42] Under our experimental conditions, the reduction of GO in an aqueous H_3PO_2 and I_2 solution produced chemically reduced GO (rGO) wet-gel, and it was freeze-dried to produce the 3D GA.

The key step in the fabrication of highly deformable GAs is to selectively adhere viscoelastic segments to the graphene sheet junctions (Fig. 1a). Under our experimental conditions, PDMS was chosen as a viscoelastic component, which had to be attached to the intersheet joints of the GA because of its high elasticity (represented by an elastic modulus of 1.8 MPa and elongations of up to 160%).[43,44] *n*-Hexane (with a solubility parameter (δ) value of 7.24 $cal^{1/2}$ $cm^{-3/2}$) was selected as a solvent for PDMS (with a δ value of 7.30 $cal^{1/2}$ $cm^{-3/2}$ in organic solvents) because of its compatibility resulting from the similar value of the solubility parameter (δ).[45,46] The close match between the corresponding solubility parameters of PDMS and *n*-hexane produces a transparent diluted PDMS solution characterized by good mixing and processability. Most importantly, the quasi-plastic nature of the GAs originates from the surface tension and capillary forces of diluted PDMS solutions.

As illustrated in Fig. 1b, the PDMS components were able to approach and selectively bond to the graphene sheet junc-

Published on 19 May 2016. Downloaded by MIT Library on 27/06/2017 20:37:01.

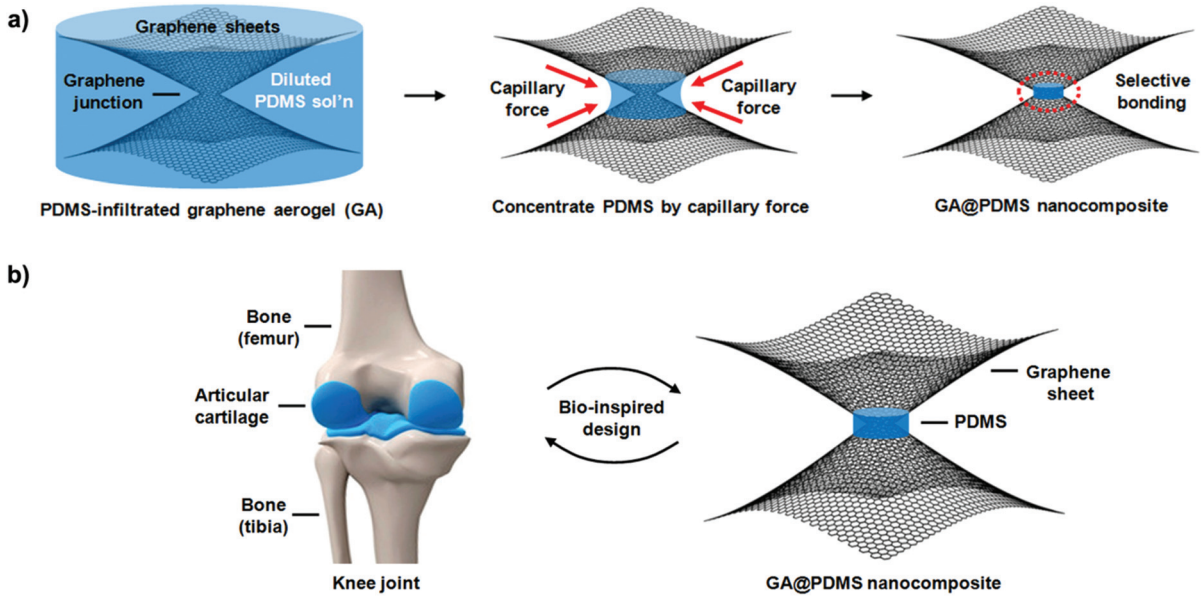

Fig. 1 (a) A schematic illustration of the cartilage principle and cartilage-inspired artificial design of the superelastic and tough 3D GAs prepared by selective bonding of soft PDMS to hard graphene sheet junctions. (b) A schematic representation of the articular cartilage and cartilage-inspired GA. The bones (femur and tibia) are joined together by the articular cartilage.

tions, which resemble soft cartilages attached to hard bone joints. PDMS bonding to the rGO intersheet joints will be discussed in detail below.

In order to characterize the pore structure of the obtained GA@PDMS nanocomposite, scanning electron microscopy (SEM) measurements were performed. The monolithic GA@PDMS nanocomposite exhibited a 3D uniformly interconnected macroporous structure (Fig. 2a) with pore characteristics similar to those for pristine GAs, while typical structural shrinkage was not observed. Thus, the introduction of the PDMS component, which strongly interacts with the intersheet junctions, has little effect on the GA pore characteristics, indicating that the influence of excess polymer on the electrical conductivity of the material is almost negligible for the full utilization of graphene functionality (ESI†). The cylindrically shaped GA@PDMS nanocomposite was produced using a one-batch reaction on a scale of several cm, which represents a very large quantity for laboratory-scale production (Fig. 2a, inset). The as-prepared GA@PDMS nanocomposite showed the lowest bulk density of 18.5 mg cm^{-3}. The continuously interconnected macropores had diameters ranging from 5 to 15 μm, while the pore walls were composed of single or few layers of graphene sheets, as confirmed by the enlarged SEM images (Fig. 2b and inset).

To investigate the pore characteristics of the GA@PDMS nanocomposites, nitrogen sorption measurement was conducted (ESI†). Interestingly, there is no significant difference between the pristine GA and GA@PDMS nanocomposite. They exhibit similar pore features (*e.g.* types of adsorption/desorption isotherms and pore volume). The surface areas of the pristine GA and GA@PDMS nanocomposite, which were calculated by the BET equation using N_2 adsorption/desorption isotherms, were also estimated to be 302.4 m^2 g^{-1} and 293.2 m^2 g^{-1}, respectively. From the BJH pore size distribution, it was also observed that the GA@PDMS nanocomposite has a pore volume of 1.45 cm^3 g^{-1} with a pore diameter in the range of about 10 to 200 nm. This result is almost the same as the value of pristine GA before PDMS introduction (pore volume of 1.48 cm^3 g^{-1}).

The important features of the produced GA@PDMS nanocomposite are its superelastic properties and high compressive mechanical strength, as shown in Fig. 2c. The obtained monolithic sample was robust enough to withstand severe and repeated bending and/or compression.

The existence and distribution of the PDMS component in the GA were characterized by the obtained elemental mapping images of energy dispersive spectrometry (EDS). Fig. 2d clearly shows that carbon (C) elements are widely distributed throughout the whole graphene sheet surface, while most silicon (Si) atoms are localized at the graphene sheet junctions, indicating selective bond formations. The EDS analysis also revealed the presence of C (73.7%), O (23.55%), and Si (2.76%) elements, which confirmed that small PDMS amounts were effectively anchored to the 3D graphene networks.

The presence of PDMS in the GA was quantitatively investigated by thermogravimetric analysis (TGA). The TGA thermograms of PDMS, the GA, and the GA@PDMS nanocomposite are shown in Fig. 3a. Their corresponding residual weights (or char yields) at 800 °C were estimated to be 40.1%, 85.1%, and 82.9%, respectively. The mass fraction of the PDMS com-

 This journal is © The Royal Society of Chemistry 2016

Published on 19 May 2016. Downloaded by MIT Library on 27/06/2017 20:37:01.

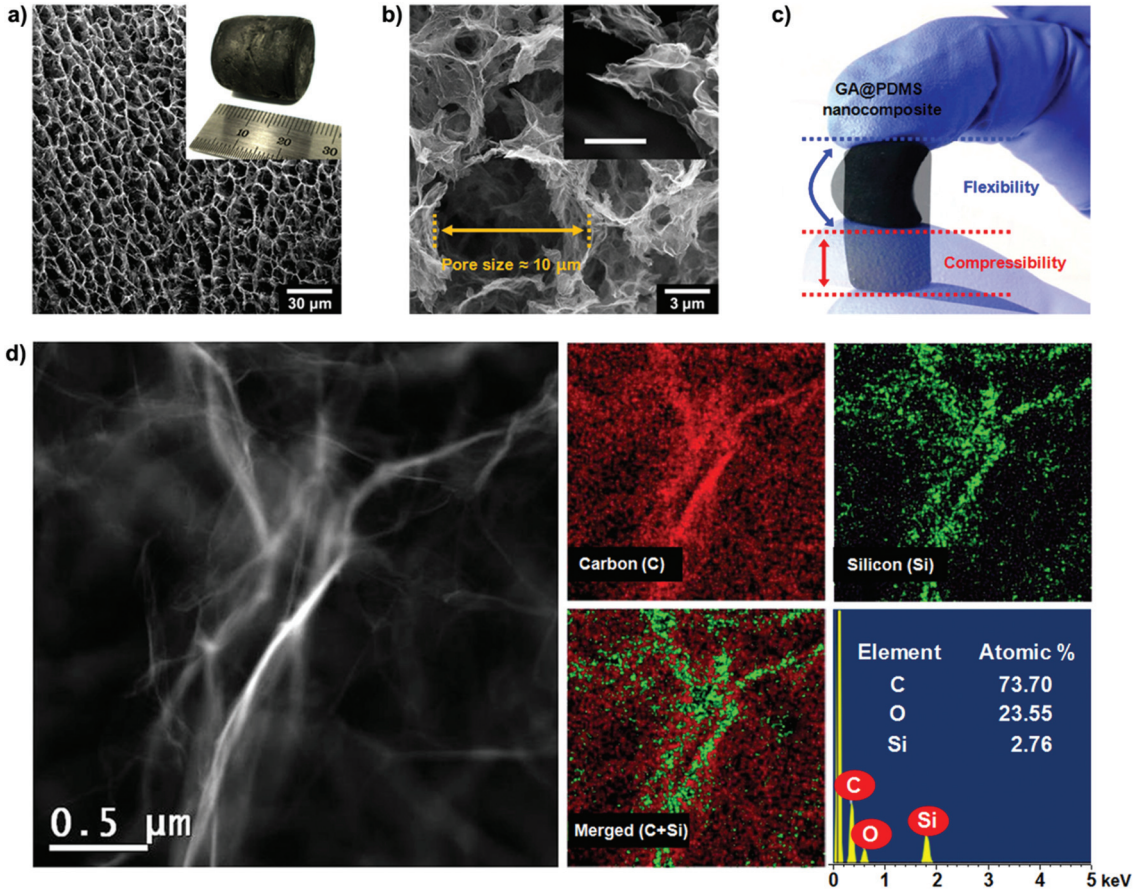

Fig. 2 (a) An SEM image of the resulting GA@PDMS nanocomposite at low magnification. A digital image (inset) showing a centimeter-sized GA@PDMS nanocomposite obtained by a single-reaction step. (b) An SEM image of the GA@PDMS nanocomposite at high magnification. The GA@PDMS nanocomposite exhibits uniformly interconnected pores with average sizes of around 10 μm (the inset scale bar is 100 nm). (c) A photograph of the GA@PDMS nanocomposite, which shows its flexibility and compressibility. (d) HAADF-STEM image/EDS mapping results for carbon (C) and silicon (Si) elements, and their merged image (C + Si), and the EDS analysis of the selected area of the GA@PDMS nanocomposite surface.

ponent in the GA@PDMS nanocomposite was calculated as follows: PDMS content = (17.1% − 14.9%)/(0.6 − 0.15) = 4.8%. Therefore, the stoichiometric percent composition of the PDMS component in the GA@PDMS was equal to 4.8%.

In order to achieve an in-depth insight into the chemical structure and interactions of the GA@PDMS nanocomposite, spectroscopic analyses were performed using Fourier transform infrared (FT-IR) spectroscopy, Raman spectroscopy, and X-ray photoelectron spectroscopy (XPS). In comparison with the FT-IR features of the pristine GA, the PDMS spectrum exhibited IR peaks at 789–796 cm^{-1}, 1020–1074 cm^{-1}, and 1255–1259 cm^{-1}, which were assigned to the $-CH_3$ rocking and Si–C stretching in Si–CH_3, Si–O–Si stretching, and CH_3 deformation in Si–CH_3, respectively (Fig. 3b).[47,48] As expected, the GA@PDMS nanocomposite showed the distinct IR features of pristine PDMS, which could not be obtained for the pristine GA. The observed band discrepancy and appearance of the new peaks originated from the chemical interaction of PDMS with oxygen-containing functional groups of the GA junctions.

Raman spectroscopy measurements were conducted to confirm the structural evolution of the GA and quantify the crystallinity of the PDMS segments (Fig. 3c). The pristine GA exhibited a typical Raman spectrum with two distinct D- and G-bands at 1340 and 1594 cm^{-1}, respectively, and a ratio of the integrated peak intensities (I_D/I_G) of 1.49.[49,50] The GA@PDMS nanocomposite was characterized by the same peak positions and a similar I_D/I_G value of 1.51, suggesting the absence of significant changes in the GA electronic structure due to the marginal inclusion of PDMS into the intersheet junctions. Interestingly, the sharp and strong PDMS peak at 495 cm^{-1} (Si–O–Si stretching) tends to weaken, broaden, and shift to lower wavenumbers (around 455 cm^{-1}) for the GA@PDMS nanocomposite (Fig. 3c inset). Such a phenomenon can be related to the GA degree of crystallinity. PDMS is a practically semi-crystalline polymer, and its crystallinity is influenced by many factors (such as molecular weight, molecular structure, and nucleation). Under the experimental conditions described in this work, the crystallization process of diluted PDMS near graphene sheet junctions is impeded due to the geometrical

Published on 19 May 2016. Downloaded by MIT Library on 27/06/2017 20:37:01.

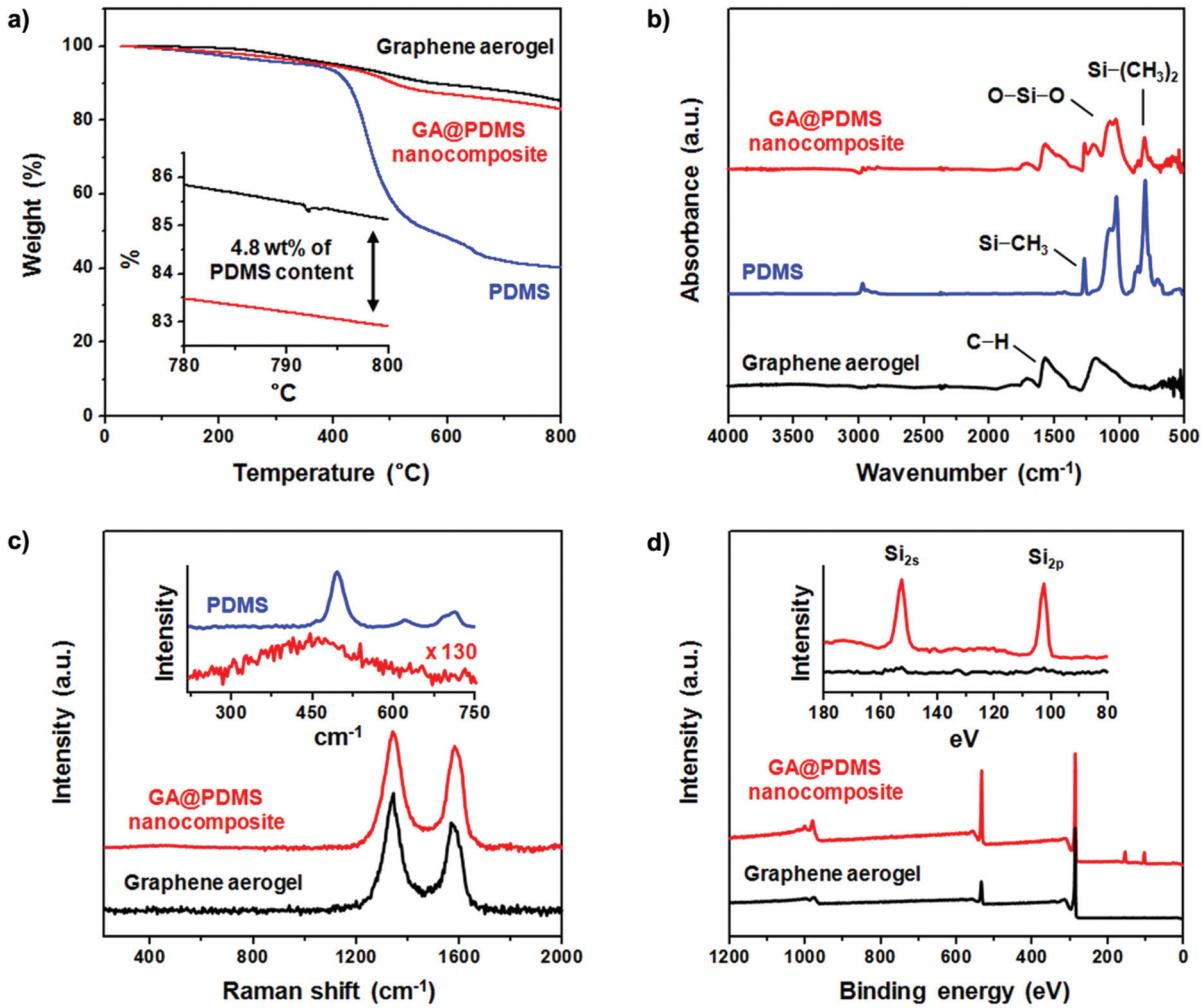

Fig. 3 (a) Thermogravimetric analysis results for PDMS, the GA, and the GA@PDMS nanocomposite, respectively. The inset on the right side shows the enlarged end of the TGA curve. (b) FT-IR spectra of PDMS, the GA, and the GA@PDMS nanocomposite, respectively. (c) 532 nm excited Raman spectra of the GA and GA@PDMS nanocomposite. (d) A full-range XPS survey of the GA and GA@PDMS nanocomposite (inset: the XPS Si_{2s} and Si_{2p} spectra of the GA and GA@PDMS nanocomposite).

constraints originating from the chain dynamics. When crystallization is induced by the confined geometry of nanoscale intersheets, the chain mobility is significantly suppressed, leading to a reduction in the degree of crystallinity.[51]

XPS survey scanning is an effective way to determine the presence of C, O, and Si elements on the GA surface and to obtain the related atomic percentages. The general survey spectra and high-resolution spectra for the GA and GA@PDMS nanocomposites are shown in Fig. 3d. Successful PDMS bonding was verified by the appearance of the Si_{2p} and Si_{2s} peaks at 102 and 153 eV, respectively, while no peaks corresponding to the Si species were observed for the pristine GA sample above the XPS detection limit (Fig. 3d inset). In addition, the elemental compositions of the GA and GA@PDMS nanocomposite were determined from the corresponding XPS peak areas and corrected by their respective atomic sensitivity factors. The full range survey scan for the pristine GA provided the composition of C (79.85%), O (10.91%), and N (0.1%), which is consistent with the results previously obtained for conventional chemically reduced graphene samples. In contrast, the GA@PDMS nanocomposite had the composition of C (76.72%), O (13.55%), and Si (2.76%) with a relatively high O content due to the presence of PDMS siloxane groups (Si–O–Si).

According to the obtained spectroscopic results, it can be concluded that the PDMS components were selectively incorporated into the intersheet joints of the GA through capillary forces and effectively reinforced its brittle network *via* chemical interactions while preserving intrinsic electronic conduction pathways (ESI†).

Comparison between mechanical properties of GA and GA@PDMS nanocomposite

As shown in Fig. 4a and b, the mechanical integrity of the GA and GA@PDMS nanocomposite was investigated by uniaxial compression measurements performed using a strain-con-

 This journal is © The Royal Society of Chemistry 2016

Published on 19 May 2016. Downloaded by MIT Library on 27/06/2017 20:37:01.

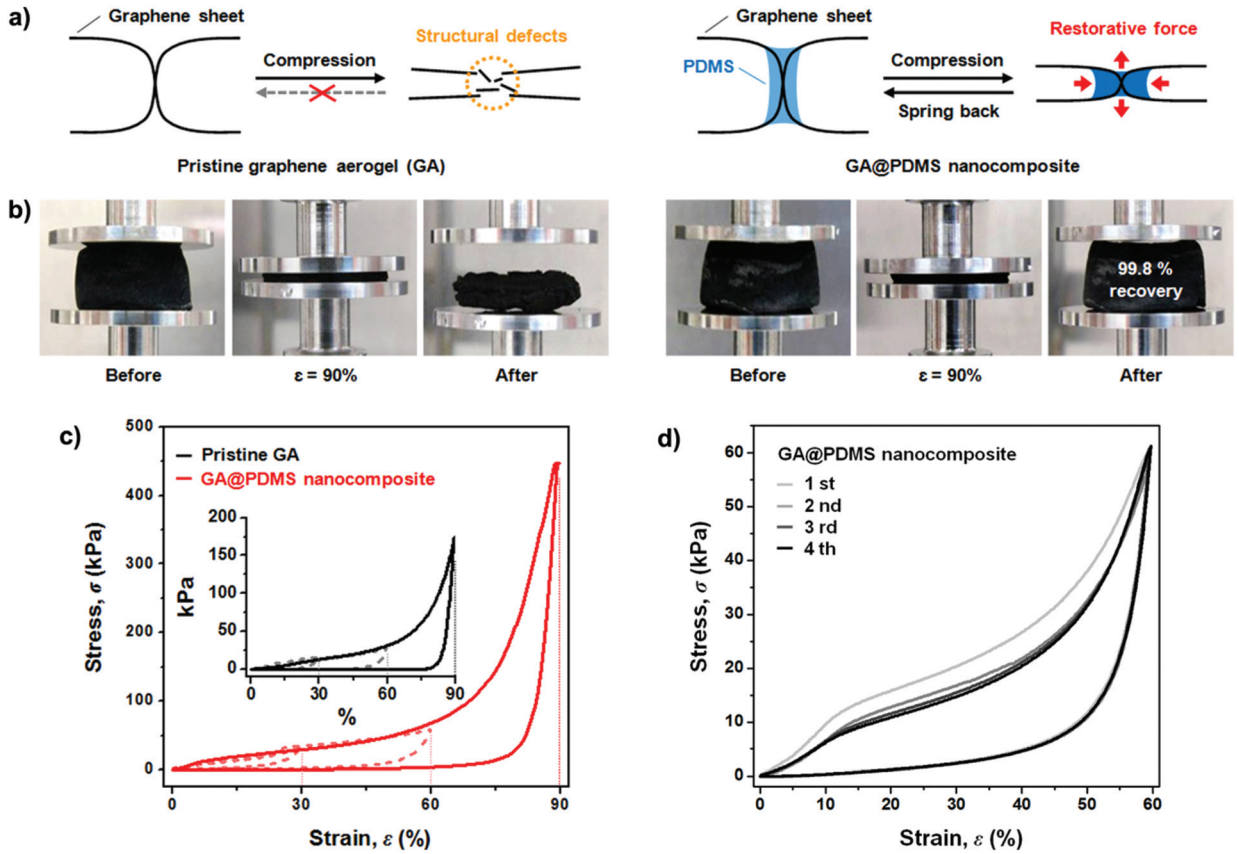

Fig. 4 (a) Roles of selectively bonded PDMS segments in GAs under compressive strain. (b) Digital photographs of the GA and GA@PDMS nanocomposite after compression at a strain of 90%. (c) Compressive stress–strain curves plotted for the GA (black) and GA@PDMS nanocomposite (red) at compressive strains of 30, 60, and 90%. (d) Compressive stress–strain curves for the GA@PDMS nanocomposite obtained using repeated cycles by the dynamic mechanical analyzer at a 60% strain and uniaxial compression.

trolled dynamic mechanical analyzer equipped with parallel plates (TA Instruments, RSA3). Note that the mechanical properties of both aerogels were tested under dry ambient conditions. The maximum compressive strength increased with higher applied strains of 30, 60, and 90% (inset of Fig. 4c). At an applied strain of 90%, 174.0 kPa of compressive stress was measured for the pristine GA. An elastic modulus value of 42.7 kPa was obtained from the unloading curve by using the initial linear slope. As was expected, weak van der Waals intermolecular interactions at the graphene sheet junctions were unable to produce a reversible recovery of the GA at a compressive strain of 90%. During the unloading process, the compressive stress reached zero value at a strain of 71.4% indicating that the GA recovery kinetics is slower than the unloading rate of the parallel plate fixture (3 mm min^{-1}). After the complete removal of the applied strain, 57% of the original height was recovered (rather than 29%).

The selective insertion of PDMS into the GA junctions dramatically modified the related GA mechanical properties. Intersheet junctions in pristine GAs act as structural defects, which determine the overall strength of the GA networks. The compressive strength of the GA@PDMS nanocomposite increased from 174.0 kPa to 448.2 kPa at an applied strain of 90% because the structural defects at the intersheet junctions were strengthened by the covalently bonded PDMS. Such viscoelastic soft segments can dissipate energy (damping) and effectively transfer loads leading to a two-fold increase of the initial elastic modulus value (87.7 kPa). In addition, the PDMS components also play the role of a lubricant that has both anti-adherent and glidant properties. During the loading/unloading processes, this PDMS component could be hampering the chances of graphene sheet agglomeration and restacking. Thus, a remarkable recovery rate (99.8% of the original height) was achieved after the complete removal of the applied strain (90%).

According to the unloading curve with a compressive strain of 90%, a zero stress value was reached at a 14.1% strain corresponding to the 85.9% recovery of the GA@PDMS nanocomposite. This observation demonstrates significantly enhanced recovery (compared to the 28.6% recovery of the pristine GA). Remarkably, reversible ultraelastic mechanical properties were achieved for the GA@PDMS nanocomposite through the repeated cycles of a 60% applied strain (Fig. 4d).

Furthermore, the dynamic response to applied forces and structural transformation/recovery are important factors that

Published on 19 May 2016. Downloaded by MIT Library on 27/06/2017 20:37:01.

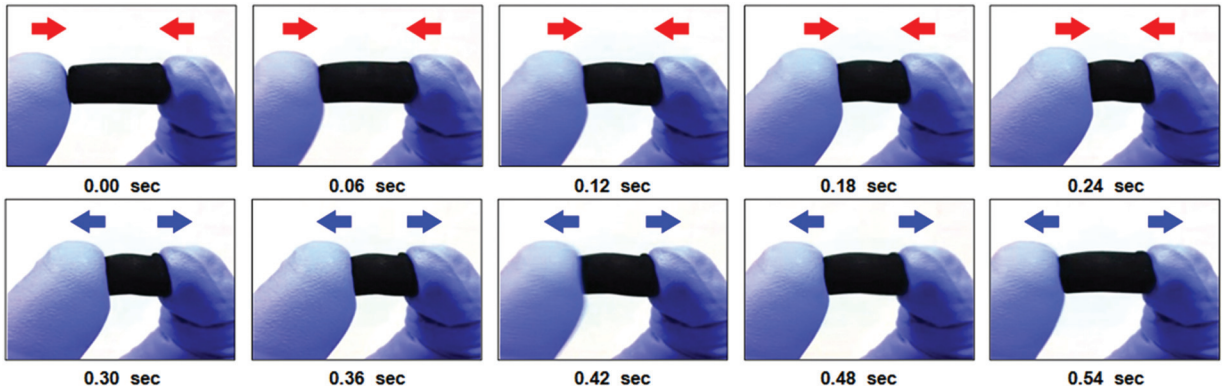

Fig. 5 A compression test conducted using fingers. The thumb and index fingers pressed the GA@PDMS nanocomposite at a compressive strain of about 40%.

determine the material performance and lifetime. Fig. 5 describes a series of compression tests conducted for the produced GAs. The obtained real-time captured images clearly indicate that the GA@PDMS nanocomposite was instantly transformed along the stress direction (upper row) and then immediately recovered its original shape (bottom row) within a few ms, thus exhibiting relaxation on a shorter timescale (ESI Movie S1†).

The simultaneous improvement in both stress and recovery properties suggests increased energy-to-break (or toughness) values, which often uniquely characterize nanocomposites, containing less than 10 wt% of rigid fillers dispersed over polymer matrices. In this study, an inversed nanocomposite strategy was adopted by using 99.5 wt% of filler-like hard graphene nanosheets bonded to extremely small amounts (0.5 wt%) of soft PDMS. We have also tested various weight

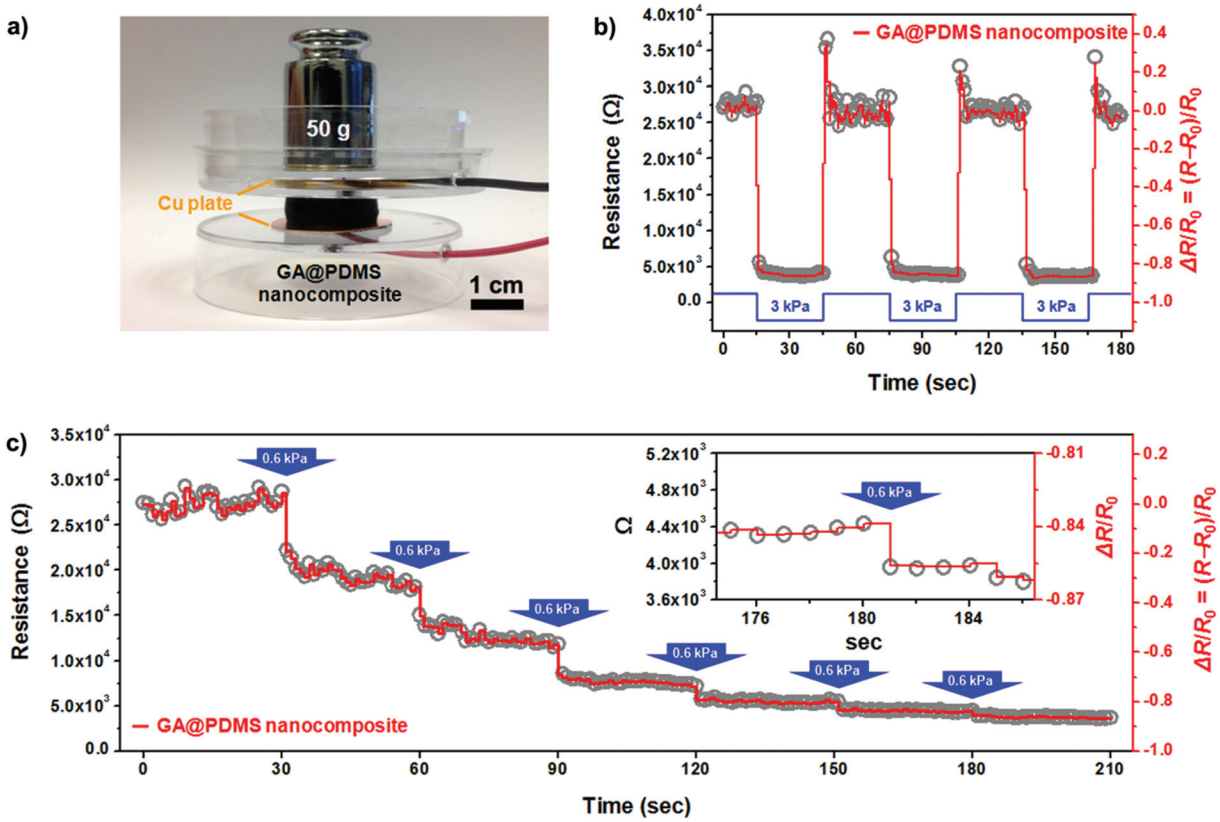

Fig. 6 (a) A digital photograph of the proposed strain sensor. (b) Real-time responses of the GA@PDMS nanocomposite under repetitive loading pressure (3.0 kPa). The resistance values were monitored at a constant voltage value (0.1 V). (c) Variations in resistance (grey circles) and normalized resistance changes (red line) for the GA@PDMS nanocomposite upon sequentially applied pressure (0.6, 1.2, 1.8, 2.4, 3.0, and 3.6 kPa).

 This journal is © The Royal Society of Chemistry 2016

Published on 19 May 2016. Downloaded by MIT Library on 27/06/2017 20:37:01.

fractions of PDMS (0.1, 0.5, 1.0, 3.0 and 5.0 wt%) to optimize the required PDMS content (ESI†). Until reaching the optimum PDMS concentration of 0.5 wt%, both the modulus and compressive strength increased due to the effective load transfer *via* the PDMS junction. However, excessive PDMS turned out to be deleterious to the mechanical properties of the aerogel. This is somewhat analogous to the reinforcement of polymer nanocomposites. In the case of nanocomposites, mechanical reinforcement can be greater than the rule of mixture, when the optimum filler loading amount by strong polymer–particle interaction as well as large interfacial area to volume ratio is achieved. However, the inclusion of additional nanoparticles causes phase separation and reduction of interfacial areas resulting in decreased mechanical strength and elongational properties. In the same manner, extra PDMS cannot stay only at the graphene intersheet junctions that are interfaced between graphene and PDMS. As a result, the composite containing 0.5 wt% of PDMS exhibited the best mechanical properties.

Due to the combination of excellent compressibility with good electrical conductivity, the obtained GA@PDMS nanocomposites can be utilized in strain sensors. To demonstrate their potential applications as signal transducers, the GA@PDMS nanocomposites were placed between two copper electrodes, and their electrical responses were monitored in real time (Fig. 6a). To obtain reliable test results, the samples were pre-treated by applying a 50% strain several times until they exhibited a steady resistance response.

To evaluate the real-time responses of the GA@PDMS nanocomposites, their electrical resistance was monitored in real time during each loading step of 100 g. The GA@PDMS nanocomposites exhibited conductivities in the range of about $(0.4–25) \times 10^{-2}$ S m^{-1}, which is comparable to the conductivity values for GAs reported in the literature.[52–57] Fig. 6b depicts the symmetrical curves obtained during loading/unloading. When a load was applied, the resistance values decreased instantaneously. In contrast, the resistance values rapidly recovered to their original levels (>98%) when the applied load was removed, exhibiting the reversibility and reproducibility properties. The observed change in electrical resistance with an applied force can be elucidated by the proximate contact of individual graphene sheets bridged by chemically bonded PDMS species.[58] In fact, when GAs are used in electrodes, the effective conducting path is of primary importance. The GAs do not exhibit good conductivity if the contact resistance between individual graphene sheets is too high. Our observations suggest that the contact resistance can be reduced by overlapping graphene sheets in GA conducting networks. The introduction of applied forces causes the formation of new conductive paths and/or redistribution of the existing ones, thus triggering better contacts and further reduction in the electrical resistance. In addition, the GA@PDMS nanocomposites were characterized by very short response (t_{res}) and recovery times (t_{rec}) (defined as the time required for the response or recovery to change from 0% to 90% of its final value). It should be noted that the GA@PDMS nanocomposites exhibit very small t_{res} and t_{rec} values (in the millisecond range), which are closely related to the intrinsic characteristics of the selectively bonded PDMS segments.

The electrical fatigue and resistance response of the GA@PDMS nanocomposites to sequential loading are described in Fig. 6c (ESI Movie S2†). The electrical fatigue was calculated by measuring the sheet resistance change, $\Delta R/R_0 = (R - R_0)/R_0$, where R and R_0 are the resistance response induced by loading and the initial resistance of the sample, respectively. The sensing signals ($\Delta R/R_0$) were characterized by high sensitivity and rapid response times at different loading amounts (20, 40, 60, 80, 100, and 120 g), indicating that the GA@PDMS nanocomposites can also be used as strain sensors.

The sensitivity (defined as $\Delta R/R_0 \times 100\%$) was calculated from the measured resistance values and plotted as a function of the applied force (for total 10 measured samples). As displayed in Fig. 7a, an inversely proportional relationship between the sensitivity and the applied force was clearly observed for all studied samples. When the force value was 0.2 N, the corresponding sensitivity was equal to around −36%. A further increase in the applied force resulted in an

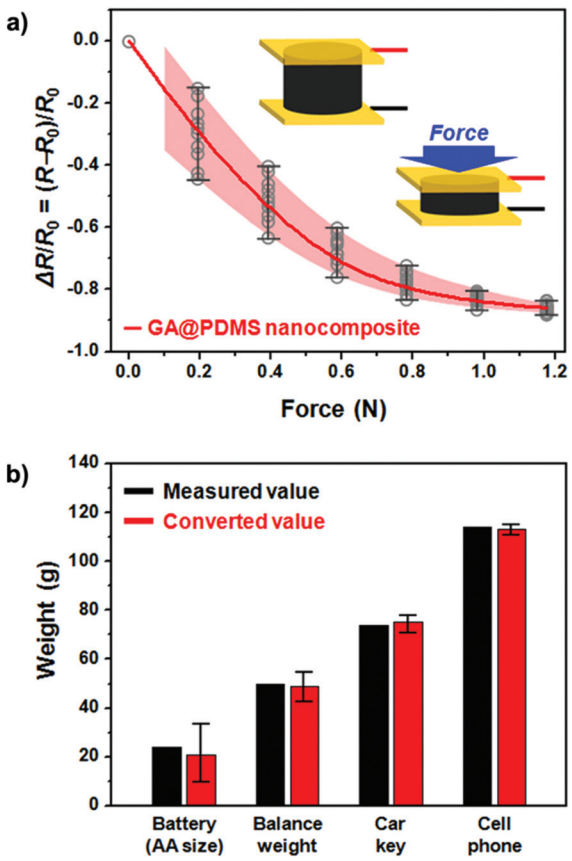

Fig. 7 (a) Sensitivity changes for the GA@PDMS nanocomposite as functions of various forces (0.196, 0.392, 0.588, 0.784, 0.98, and 1.176 N). Total 10 samples were measured and plotted. (b) A comparison between the measured and converted weight values for the representative objects.

Published on 19 May 2016. Downloaded by MIT Library on 27/06/2017 20:37:01.

increase in sensitivity, reaching −86% at 1.2 N and −87% at forces greater than 1.3 N.

It is important to note that the non-linear curve fit (denoted in Fig. 7a by the red line) provides a 'universal curve' of the sensitivity (%) *versus* force (N). Although the initial resistances are different for each sample, the electrical fatigue ($\Delta R/R_0$) distributions exhibit the same tendencies. Therefore, if the $\Delta R/R_0$ is measured at a certain force (mass × acceleration), it is possible to estimate the unknown mass from the 'universal curve' by interpolation.

To investigate the possibility of using the proposed system in electronic scales, four representative things (an AA-sized battery, a balance weight, a car key, and a cell phone) were selected and used as items of unknown mass. Interestingly, the converted values interpolated from the calibration curve were very close to the measured ones (Fig. 7b). For the sample with a diameter of 1.72 cm, height of 0.78 cm, and weight of 0.26 g, the maximum detectable weight was 120 g, which was about 4600 times greater than its real weight.

Conclusions

In summary, a facile and innovative composite strategy has been proposed to fabricate GA@PDMS nanocomposites, in which PDMS segments are selectively attached to GA junctions. The cartilage-inspired, selectively bonded viscoelastic PDMS components provide the restorative force (acting as springs) that converts fragile 3D graphene networks into superelastic and ultradurable 3D GAs. Consequently, the GA@PDMS nanocomposites exhibit reversible structural deformations (corresponding to an almost 100% recovery of the original height at a compressive strain of 90%) with rapid response and recovery rates (millisecond scale) and high compressive mechanical strength (448.2 kPa at a compressive strain of 90%) over repeated compression cycles due to the energy dissipation and transfer of applied forces. The GA@PDMS nanocomposites also demonstrate remarkable electrical performance (corresponding to a maximum conductivity of 25×10^{-2} S m^{-1}), while variations in their resistance are inversely proportional to the applied forces. Thus, the GA@PDMS nanocomposites can be used as signal transducers in strain sensors owing to their reliable sensitivity and excellent durability. Due to their outstanding mechanical/electrical properties, the GA@PDMS nanocomposites may pave the way to various practical applications that include sensors, actuators, and materials for flexible devices. Furthermore, our proposed concept can be extended to fabricate other multifunctional nanocomposites by introducing additional functional components into monolithic structures.

Acknowledgements

We would like to acknowledge the financial support from the R&D Convergence Program of NST (National Research Council of Science & Technology) of Republic of Korea and the Energy Efficiency & Resources program of the Korea Institute of Energy Technology Evaluation Planning (KETEP) granted financial resources from the Ministry of Trade, Industry & Energy, Republic of Korea (No. 20122010100140). Dr. Hong was supported by the AFOSR FATE MURI, Grant No. FA9550–15–1–0514, the STC Center for Integrated Quantum Materials (CIQM) from NSF (US) grant DMR-1231319, and Army Research Office (ARO) (Grants W911NF-14-2-0071, 6930265 and 6930861).

Notes and references

1 J. L. Suter, D. Groen and P. V. Coveney, *Adv. Mater.*, 2015, **27**, 966–984.
2 X. Huang and P. Jiang, *Adv. Mater.*, 2015, **27**, 546–554.
3 N. Jouault, D. Lee, D. Zhao and S. K. Kumar, *Adv. Mater.*, 2014, **26**, 4031–4036.
4 N. Yousefi, X. Sun, X. Lin, X. Shen, J. Jia, B. Zhang, B. Tang, M. Chan and J.-K. Kim, *Adv. Mater.*, 2014, **26**, 5480–5487.
5 J. Wang, Q. Cheng and Z. Tang, *Chem. Soc. Rev.*, 2012, **41**, 1111–1129.
6 J. R. Potts, D. R. Dreyer, C. W. Bielawski and R. S. Ruoff, *Polymer*, 2011, **52**, 5–25.
7 P. Das, J.-M. Malho, K. Rahimi, F. H. Schacher, B. Wang, D. E. Demco and A. Walther, *Nat. Commun.*, 2015, **6**, 5967.
8 H.-B. Yao, J. Ge, L.-B. Mao, Y.-X. Yan and S.-H. Yu, *Adv. Mater.*, 2014, **26**, 163–188.
9 H. Kakisawa and T. Sumitomo, *Sci. Technol. Adv. Mater.*, 2011, **12**, 064710.
10 H. D. Espinosa, J. E. Rim, F. Barthelat and M. J. Buehler, *Prog. Mater. Sci.*, 2009, **54**, 1059–1100.
11 S. Wan, Y. Li, J. Peng, H. Hu, Q. Cheng and L. Jiang, *ACS Nano*, 2015, **9**, 708–714.
12 P. Das, J.-M. Malho, K. Rahimi, F. H. Schacher, B. Wang, D. E. Demco and A. Walther, *Nat. Commun.*, 2015, **6**, 5967.
13 Q. Cheng, J. Duan, Q. Zhang and L. Jiang, *ACS Nano*, 2015, **9**, 2231–2234.
14 Y.-Q. Li, T. Yu, T.-Y. Yang, L.-X. Zheng and K. Liao, *Adv. Mater.*, 2012, **24**, 3426–3431.
15 J.-Y. Hong, J. J. Wie, Y. Xu and H. S. Park, *Phys. Chem. Chem. Phys.*, 2015, **17**, 30946–30962.
16 S. Yun, S.-O. Kang, S. Park and H. S. Park, *Nanoscale*, 2014, **6**, 5296–5302.
17 B. C. Kim, J.-Y. Hong, G. G. Wallace and H. S. Park, *Adv. Energy Mater.*, 2015, **5**, 1500959.
18 S. Nardecchia, D. Carriazo, M. L. Ferrer, M. C. Gutiérrez and F. D. Monte, *Chem. Soc. Rev.*, 2013, **42**, 794–830.
19 H. Jiang, P. S. Lee and C. Z. Li, *Energy Environ. Sci.*, 2013, **6**, 41–53.
20 Q. Peng, Y. Li, X. He, X. Gui, Y. Shang, C. Wang, C. Wang, W. Zhao, S. Du, E. Shi, P. Li, D. Wu and A. Cao, *Adv. Mater.*, 2014, **26**, 3241–3247.
21 V. Chabot, D. Higgins, A. Yu, X. Xiao, Z. Chena and J. Zhang, *Energy Environ. Sci.*, 2014, **7**, 1564–1596.

 This journal is © The Royal Society of Chemistry 2016

Published on 19 May 2016. Downloaded by MIT Library on 27/06/2017 20:37:01.

22 M. D. Stoller, S. Park, Y. Zhu, J. An and R. S. Ruoff, *Nano Lett.*, 2008, **8**, 3498–3502.
23 C. Liu, Z. Yu, D. Neff and A. Zhamu, *Nano Lett.*, 2010, **10**, 4863–4868.
24 S. Han, D. Wu, S. Li, F. Zhang and X. Feng, *Adv. Mater.*, 2014, **26**, 849–864.
25 H. Huang, P. Chen, X. Zhang, Y. Lu and W. Zhan, *Small*, 2013, **9**, 1397–1404.
26 X. Zhang, Z. Sui, B. Xu, S. Yue, Y. Luo, W. Zhan and B. Liu, *J. Mater. Chem.*, 2011, **21**, 6494–6497.
27 K. H. Kim, Y. Oh and M. F. Islam, *Nat. Nanotechnol.*, 2012, **7**, 562–566.
28 C. Zhu, T. Y.-J. Han, E. B. Duoss, A. M. Golobic, J. D. Kuntz, C. M. Spadaccini and M. A. Worsley, *Nat. Commun.*, 2015, **6**, 6962.
29 Y. Zhao, J. Liu, Y. Hu, H. Cheng, C. Hu, C. Jiang, L. Jiang, A. Cao and L. Qu, *Adv. Mater.*, 2013, **25**, 591–595.
30 S. Ye and J. Feng, *ACS Appl. Mater. Interfaces*, 2014, **6**, 9671–9679.
31 J.-Y. Hong, B. M. Bak, J. J. Wie, J. Kong and H. S. Park, *Adv. Funct. Mater.*, 2015, **25**, 1053–1062.
32 H. Ha, K. Shanmuganathan and C. J. Ellison, *ACS Appl. Mater. Interfaces*, 2015, **7**, 6220–6229.
33 Z. Chen, W. Ren, L. Gao, B. Liu, S. Pei and H.-M. Cheng, *Nat. Mater.*, 2011, **10**, 424–428.
34 Y. A. Samad, Y. Li, S. M. Alhassan and K. Liao, *ACS Appl. Mater. Interfaces*, 2015, **7**, 9195–9202.
35 X. Wang, Y. Zhang, C. Zhi, X. Wang, D. Tang, Y. Xu, Q. Weng, X. Jiang, M. Mitome, D. Golberg and Y. Bando, *Nat. Commun.*, 2013, **4**, 2905.
36 I. K. Moon, J. Lee, R. S. Ruoff and H. Lee, *Nat. Commun.*, 2010, **1**, 73.
37 J. Zhao, S. Pei, W. Ren, L. Gao and H.-M. Cheng, *ACS Nano*, 2010, **4**, 5245–5252.
38 Y. Xu, Q. Wu, Y. Sun, H. Bai and G. Shi, *ACS Nano*, 2010, **4**, 7358–7362.
39 Y. Xu, K. Sheng, C. Li and G. Shi, *ACS Nano*, 2010, **4**, 4324–4330.
40 H. Bi, K. Yin, X. Xie, Y. Zhou, N. Wan, F. Xu, F. Banhart, L. Sun and R. S. Ruoff, *Adv. Mater.*, 2012, **24**, 5124–5129.
41 J. Zhao, W. Ren and H.-M. Cheng, *J. Mater. Chem.*, 2012, **22**, 20197–20202.
42 H. D. Pham, V. H. Pham, T. V. Cuong, T.-D. Nguyen-Phan, J. S. Chung, E. W. Shina and S. Kim, *Chem. Commun.*, 2011, **47**, 9672–9674.
43 H. E. Jeong and K. Y. Suh, *Lab Chip*, 2008, **8**, 1787–1792.
44 C. Y. Hui, A. Jagota, Y. Y. Lin and E. J. Kramer, *Langmuir*, 2002, **18**, 1394–1407.
45 J. N. Lee, C. Park and G. M. Whitesides, *Anal. Chem.*, 2003, **75**, 6544–6554.
46 S. Lee, H. Jeon, M. Jang, K.-Y. Baek and H. Yang, *ACS Appl. Mater. Interfaces*, 2015, **7**, 1290–1297.
47 L. M. Johnson, L. Gao, C. W. Shields IV, M. Smith, K. Efimenko, K. Cushing, J. Genzer and G. P. López, *J. Nanobiotechnol.*, 2013, **11**, 22.
48 X.-X. Zhang, B.-B. Xia, H.-P. Ye, Y.-L. Zhang, B. Xiao, L.-H. Yan, H.-B. Lv and B. Jiang, *J. Mater. Chem.*, 2012, **22**, 13132–13140.
49 J.-Y. Hong, X. Yu, B. M. Bak, C. Pang and H. S. Park, *Carbon*, 2015, **83**, 71–78.
50 J.-Y. Hong, E. H. Sohn, S. Park and H. S. Park, *Chem. Eng. J.*, 2015, **269**, 229–235.
51 T. Dollase, H. W. Spiess, M. Gottlieb and R. Yerushalmi-Rozen, *Europhys. Lett.*, 2002, **60**, 390–396.
52 Y. Qin, Q. Peng, Y. Ding, Z. Lin, C. Wang, Y. Li, F. Xu, J. Li, Y. Yuan, X. He and Y. Li, *ACS Nano*, 2015, **9**, 8933–8941.
53 H. Hu, Z. B. Zhao, W. B. Wan, Y. Gogotsi and J. S. Qiu, *Adv. Mater.*, 2013, **25**, 2219–2223.
54 L. Qiu, J. Z. Liu, S. L. Y. Chang, Y. Wu and D. Li, *Nat. Commun.*, 2012, **3**, 1241.
55 H. Sun, Z. Xu and C. Gao, *Adv. Mater.*, 2013, **25**, 2554–2560.
56 C. Wu, X. Huang, X. Wu, R. Qian and P. Jiang, *Adv. Mater.*, 2013, **25**, 5658–5662.
57 Y. Li, J. Chen, L. Huang, C. Li, J.-D. Hong and G. Shi, *Adv. Mater.*, 2014, **26**, 4789–4793.
58 M. Mohiuddin and S. V. Hoa, *Nanoscale Res. Lett.*, 2011, **6**, 419.